

# GRB 200826A: Collapse of a Thorne-Zytkow-like Object as the Aftermath of a WD-NS Coalescence

ZONGKAI PENG,<sup>1,2</sup> ZIKE LIU,<sup>1,2</sup> AND BIN-BIN ZHANG<sup>1,2</sup>

<sup>1</sup>*School of Astronomy and Space Science, Nanjing University, Nanjing 210093, China*

<sup>2</sup>*Key Laboratory of Modern Astronomy and Astrophysics (Nanjing University), Ministry of Education, China*

## ABSTRACT

The recently reported Type II Gamma-ray Burst (GRB) 200826A challenges the collapsar models by questioning how they can generate a genuinely short duration of the event. This paper proposes that the burst can originate from the collapse of a Thorne-Zytkow-like Object (TZIO). The TZIO consists of a central neutron star (NS) with a dense white dwarf (WD) material envelope and a disk, which are formed as the aftermath of a WD-NS coalescence. We found the collapse of such a TZIO can naturally explain the short duration of GRB 200826A. Furthermore, the collapse can produce a magnetar as the central object, which provides additional energy injection via magnetic dipole radiation to the ejected WD materials, causing a bump-like feature in the optical band and a shallow decay of the X-ray band. The disk wind shell induced by the TZIO at a large radius also interact with the ejected materials, which explains the “supernova bump” observed at  $\sim 28$  days.

## 1. INTRODUCTION

The long-standing two-type origins (Zhang 2011) of Gamma-ray Bursts (GRBs) has recently been challenged by some newly discovered observations, which added that a long GRB could originate from a merger-triggered core collapse (Dong et al. 2021), whereas a short GRB can originate from a magnetar giant flare (e.g., GRB 200415A; Yang et al. 2020) or an unusual collapse of a massive star (e.g., GRB 200826A; Zhang et al. 2021; Ahumada et al. 2021). In particular, Zhang et al. (2021) suggested a possibility that the intrinsically short duration of the Type-II GRB 200826A can be explained by a progenitor involved with a compact object such as a white dwarf, which supplies much denser materials to account for the short accretion timescale to match the observed short duration.

However, as pointed in Zhang et al. (2021), isolated WDs are incapable of producing GRBs; one, therefore, has to invoke a merger process between a WD and one other compact star such as a neutron star (NS) or a black hole (BH). One of such combinations, which gains increasing interest in the field, is the WD-NS merger. The WD-involved binaries have been long proposed to serve as GRB central engines (Belczynski et al. 2002;

Middleditch 2004), however, with less attention paid on how they generate short-duration GRBs.

There are two fates for a WD-NS system, which is determined by the critical mass ratio between the WD and the NS, i.e.,  $q_{\text{crit}} = M_{\text{WD}}/M_{\text{NS}}$  (Paschalidis et al. 2011b). For  $q < q_{\text{crit}} \approx 0.5$ , the WD will fill the Roche lobe slowly and undergo stable mass transfer (SMT). In this case, the WD-NS system will form an ultra-compact X-ray binary. On the other hand, for  $q > q_{\text{crit}}$ , the WD will be disrupted by the NS and will suffer unstable mass transfer (UMT). Due to a tidal disruption process caused by UMT, the NS will screw into the center of the WD. As a result, the system of the UMT case will form a Thorne-Zytkow-like object (TZIO) with a disk.

A TZIO consists of a central NS, a dense WD material envelope, and a disk. Due to the high temperature and centrifugal force, the TZIO will not collapse promptly (Paschalidis et al. 2011b). After a typical cooling timescale of several years, the system can collapse when the electron degeneracy pressure and the centrifugal force can not resist the gravitational force, resulting in a similar accretion-induced collapse process.

In this *Letter*, we propose that the collapse of a TZIO, as an aftermath of a WD-NS merger, can successfully account for the conundrum presented in GRB 200826A, including its short duration, day-scale multi-wavelength follow-up observations, and the month-scale apparent supernova bump (Ahumada et al. 2021). We present our physical picture in §2 and derive our model’s observable components as a fit-able model in §3. We then collect the

observational data and compare them with our model by performing a Monte-Carlo fit in §4. A brief summary and discussion are followed in §5.

## 2. THE PHYSICAL PICTURE

The formation and collapse of a TZIO is illustrated in Figure 1 and outlined in the following seven steps:

1. In a WD-NS system, the WD, with a mass ratio  $q > q_{\text{crit}}$ , is captured by the NS when its orbit falls within the tidal radius (Figure 1a).
2. The WD is disrupted by the NS, and the system undergoes a UMT (Figure 1b).
3. The UMT results in a TZIO with disk (Figure 1c). Numerical simulations (Paschalidis et al. 2011b) have shown that the newborn disk, formed by the WD debris, is about the same the size of the Roche limit, and the radius of TZIO is smaller (e.g., 40% less; Paschalidis et al. 2011b) than that of the initial WD radius. Because of the shock heating during the tidal disruption process, the envelope of the newly formed TZIO as well as the disk is very hot with temperature up to  $1.5 \times 10^9$  K (Paschalidis et al. 2011b).
4. The disk is quickly accreted by the central TZIO, forming a more massive TZIO and a disk wind shell (Figure 1c,d). The two characteristic timescaled dominating the accretion process are the viscous timescale ( $t_{\text{vis}}$ ) or Alfvén timescale ( $t_A$ ), whichever is longer. These timescales are calculated by (Paschalidis et al. 2011a,b):

$$t_{\text{vis}} \simeq 53 \text{ s} \left(\frac{\alpha}{0.1}\right)^{-1} \left(\frac{H/R}{1.0}\right)^{-2} \left(\frac{R}{10^4 \text{ km}}\right)^{3/2} \left(\frac{M_{\text{TZ}}}{1.8M_{\odot}}\right)^{1/2}, \quad (1)$$

and

$$t_A \simeq 5 \times 10^6 \text{ s} \left(\frac{\beta}{10^{-12}}\right)^{-1/2} \left(\frac{H/R}{1.0}\right)^{-2} \left(\frac{R}{10^4 \text{ km}}\right)^{3/2} \times \left(\frac{M_{\text{TZ}}}{1.8M_{\odot}}\right)^{1/2} \quad (2)$$

respectively, where  $\alpha$  is the viscosity constant,  $H$  is the disk thickness,  $R$  is the radius of the disk,  $M_{\text{TZ}}$  is the mass of TZIO, and  $\beta$  is the ratio of magnetic pressure to thermal pressure.  $\beta$  which is in a large range of  $\beta \sim 10^{-17} - 10^{-7}$  to account for the wide range of the WD magnetic field (Paschalidis et al. 2011b). That said, one can calculate that it is always the case that  $t_A > t_{\text{vis}}$  according to Eqs. (1)-(2). So the existence time of the

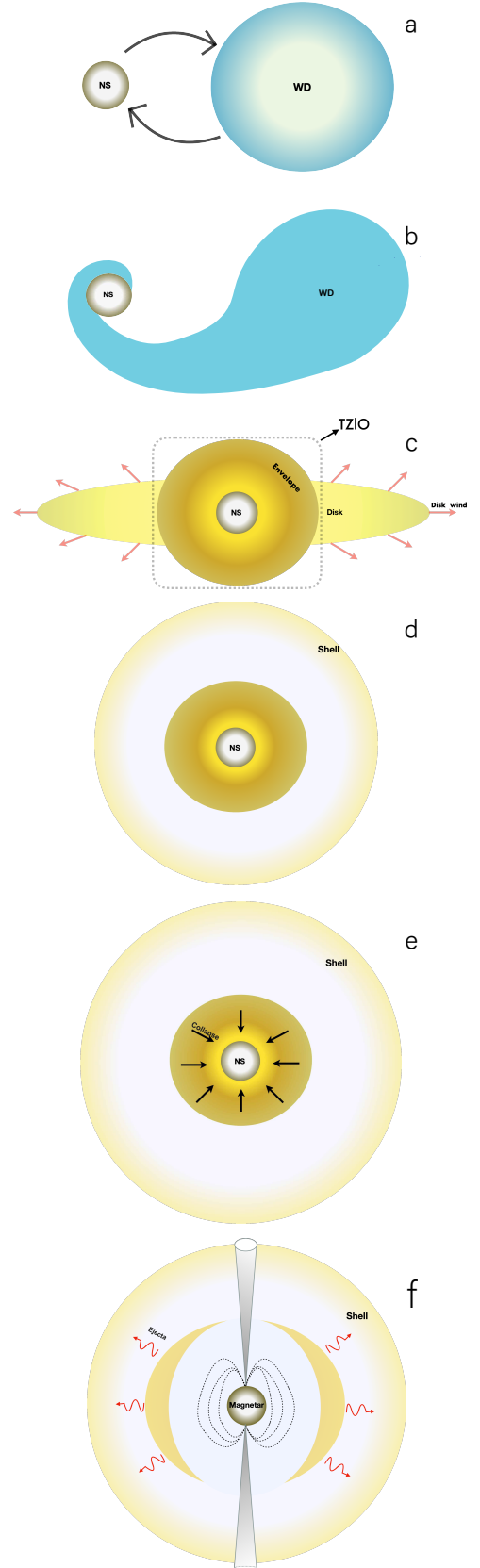


**Figure 1.** The formation and collapse of a TZIO from a WD-NS merger.

disk is dominated by the Alfvén timescale. During the accretion process, simulations also showed that 50%-80% disk mass was lost by disk wind (Margalit & Metzger 2016; Metzger 2012). The final remnant after the accretion is still a TZIO but with an increased mass contributed by 20%-50% of the WD.

The more massive TZIO then remains stable for quite a long time (Figure 1d). Assuming a mean WD density,  $\rho = 10^6 \text{ g cm}^{-3}$ , for the envelope, the calculated thermal gas pressure is about two times larger than the electron degeneracy pressure, i.e.,  $P_{\text{th}}/P_{\text{e,NR}} \approx nk_{\text{B}}T/1.0 \times 10^{13}(\rho/\mu_{\text{e}})^{5/3} \approx 1.97$ . So, initially, the envelope of TZIO is non-degenerate; the TZIO will not collapse promptly due to its high temperature and centrifugal force (Paschalidis et al. 2011b). During this period, the neutrino emission is the dominant cooling mechanism as the TZIO-disk system is in high temperature and high-density condition (Beaudet et al. 1967). The cooling timescale can be calculated as (Eqs. 73 & 74 of Paschalidis et al. 2011b)  $\tau_{\text{cooling}} \approx 1.76\rho_6/T_9^8 \text{ yr}$ .

5. After cooled down, the TZIO eventually begins to collapse (Figure 1e) when the electron degeneracy pressure of the WD envelope and the centrifugal force can not resist the gravitational force. Such an accretion-induced collapse can naturally lead to a GRB central engine (Figure 1f) which consists of a central compact object<sup>1</sup>, an accretion disk, and a relativistic jet, similar to the case of a long-GRB central engine, yet with much denser WD accreted material. The free-fall timescale of TZIO can be roughly written as

$$t_{\text{ff,TZ}} \sim \left(\frac{R_{\text{TZ}}^3}{GM_{\text{TZ}}}\right)^{1/2} \\ = 0.52 \text{ s} \left(\frac{R_{\text{TZ}}}{5 \times 10^8 \text{ cm}}\right)^{3/2} \left(\frac{M_{\text{TZ}}}{1.8 M_{\odot}}\right)^{-1/2}, \quad (3)$$

where  $G$  is the gravitational constant. Such a timescale is close to the observed duration of GRB 200826A.

6. Because of the hard shell of the NS, the collapse of the envelope (Figure 1f) will cause a rebound shock (van Riper & Lattimer 1981; van

Riper 1982). At the same time, a vast amount of neutrinos are produced by the process of electrons combined with protons to form neutrons (van Riper 1982). The rebound shock and the neutrino burst can cause part of the accreted mass to be ejected from the magnetar surface, similar to the core-collapse supernova explosions (Bruenn 1985). The ejected material can be further heated by the magnetic dipole radiation of the central magnetar and radiate as an optical bump in observation. Furthermore, the disk wind shell at a larger radius induced by the TZIO can also interact with the ejected material and produce an additional late-time bump in the optical band.

### 3. THE MODEL

One key feature of our model is that it predicts a merger-nova-like flare caused by the heated ejected material. The observed flux of such emissions can be derived as follows.

The total rotation energy of the newborn twirling magnetar in the center of TZIO (Figure 1f) is

$$E_{\text{rot}} = \frac{1}{2}I\Omega^2, \quad (4)$$

where  $I$  is the moment of inertia, and  $\Omega$  is angular velocity. The energy loss follows

$$-\frac{dE_{\text{rot}}}{dt} = -I\Omega\dot{\Omega} = \frac{B_{\text{p}}^2 R^6 \Omega^4}{6c^3} + \frac{32GI^2 \epsilon^2 \Omega^6}{5c^5} \\ = L_{\text{EM}} + L_{\text{GW}}, \quad (5)$$

which incorporates electromagnetic luminosity,  $L_{\text{EM}}$ , and gravitational wave luminosity,  $L_{\text{GW}}$ . The  $B_{\text{p}}$  corresponds to the NS surface magnetic field at the pole.  $\epsilon$  is the ellipticity of the magnetar. The time derivative of angular velocity can be described as:

$$\dot{\Omega} = -k\Omega^n, \quad (6)$$

where  $k$  can be simplified as a constant, and  $n$  is the braking index (Lasky et al. 2017). Following Yu et al. (2013); Lasky et al. (2017), we set  $n = 3$  in this work.

Combining electromagnetic part of Eq.(5) with Eq.(6), one can easily derive  $L_{\text{EM}}$  in a simple form of:

$$L_{\text{EM}} = L_0 \left(1 + \frac{t}{\tau}\right)^{-2}, \quad (7)$$

where  $L_0 = 10^{49} R_{\text{s},6}^6 B_{\text{p},15}^2 P_{0,-3}^{-4} \text{ erg s}^{-1}$  is the initial luminosity of magnetar, and  $\tau = 2 \times 10^3 R_{\text{s},6}^{-6} B_{\text{p},15}^{-2} P_{0,-3}^2 \text{ s}$  is the spin-down timescale of the magnetar. So  $L_{\text{EM}}$  can be regarded as the spin-down luminosity of the magnetar,  $L_{\text{EM}} = L_{\text{sd}}$ .

<sup>1</sup> The central object is likely a rapidly rotating magnetar (Zhong & Dai 2020) to account for the conservation of magnetic flux and angular momentum.

The total energy of the ejecta can be express as

$$E_{\text{ej}} = \Gamma M_{\text{ej}} c^2 + \Gamma E'_{\text{int}} + \Gamma^2 M_{\text{sw}} c^2, \quad (8)$$

where  $\Gamma$  is the Lorentz factor,  $E'_{\text{int}}$  is the internal energy in the comoving rest frame,  $M_{\text{sw}} = 4/3\pi R^3 n_0 m_p$  is the mass of the swept-up circum-burst medium (CBM), and  $R$  is the radius of the ejecta.

Assuming a fraction  $\xi$  of spin-down energy inject into the ejecta, one can calculate that the energy change of the eject is

$$dE_{\text{ej}} = (\xi L_{\text{sd}} - L_e) dt, \quad (9)$$

where  $L_e$  is the radiated bolometric luminosity.

The dynamical evolution of the ejecta can be written as (Huang et al. 2000; Yu et al. 2013):

$$\frac{d\Gamma}{dt} = \frac{\xi L_{\text{sd}} - L_e - \Gamma D \frac{dE'_{\text{int}}}{dt'} - (\Gamma^2 - 1) c^2 \frac{dM_{\text{sw}}}{dt}}{M_{\text{ej}} c^2 + E'_{\text{int}} + 2\Gamma M_{\text{sw}} c^2}, \quad (10)$$

where  $D = 1/[\Gamma(1 - \beta)]$  is the Doppler factor.

The variation of internal energy of the ejecta in the co-moving frame can be written as (Kasen & Bildsten 2010):

$$\frac{dE'_{\text{int}}}{dt'} = \xi \frac{L_{\text{sd}}}{D^2} - L'_e - P' \frac{dV'}{dt'}, \quad (11)$$

where the co-moving radiated luminosity is  $L'_e = L_e/D^2$ .

The last term of Eq.(11) represents the work of free expansion. In the comoving frame of the ejecta, the pressure is dominated by radiation, so

$$P' = E'_{\text{int}}/3V', \quad (12)$$

and the evolution of bulk of ejecta is

$$\frac{dV'}{dt'} = 4\pi R^2 \beta c. \quad (13)$$

By utilizing

$$\frac{dR}{dt} = \frac{\beta c}{1 - \beta}, \quad (14)$$

on can write the the co-moving radiation bolometric luminosity as (Kasen & Bildsten 2010; Kotera et al. 2013):

$$L'_e = \begin{cases} \frac{E'_{\text{int}} \Gamma c}{\tau R}, & \tau > 1 \\ \frac{E'_{\text{int}} \Gamma c}{R}, & \tau < 1, \end{cases} \quad (15)$$

where  $\tau = \kappa(M_{\text{ej}}/V')(R/\Gamma)$  is the optical depth of the ejecta, and  $\kappa$  is the opacity.

The dynamical evolution of the ejecta properties, such as  $\tau$ ,  $R$ ,  $E'_{\text{int}}$ , and  $V'$  can be solved through Eqs. (8)-(15).

For any given frequency,  $\nu$ , the observed specific flux of the ejecta can be calculated as

$$F_{\nu, \text{ej}} = \frac{1}{\max(\tau, 1)} \frac{1}{4\pi D_L^2} \frac{8\pi^2 D^2 R^2}{h^3 c^2 \nu} \frac{(h\nu/D)^4}{\exp(h\nu/DkT') - 1}, \quad (16)$$

where  $D_L$  is the luminosity distance of the burst,  $h$  is the Planck constant,  $k$  is the Boltzmann constant, and  $T' = (E'_{\text{int}}/aV')^{1/4}$  is the co-moving temperature.

In additional, the interaction between ejecta and the disk wind shell at large radius (Figure 1f) causes a forward shock and reverse shock. Such shocks heat the shell and leads to an ‘‘interaction powered SN’’ (IPSN) in optical. Following Chatzopoulos et al. (2012) and the parameterization therein, the output luminosity of the interaction can be expressed semi-analytically as:

$$\begin{aligned} L_{t, \text{IPSN}} &= \frac{1}{t_0} e^{-\frac{t}{t_0}} \int_0^t e^{\frac{t'}{t_0}} \left[ \frac{2\pi}{(n-s)^3} g^n \frac{5-s}{n-s} q^{\frac{n-5}{n-s}} (n-3)^2 \right. \\ &\quad \times (n-5) \beta_{\text{F}}^{5-s} A^{\frac{5-s}{n-s}} (t' + t_i)^{\frac{2n+6s-n-15}{n-s}} \\ &\quad \times \theta(t_{\text{FS,BO}} - t') + 2\pi \left( \frac{Ag^n}{q} \right)^{\frac{5-n}{n-s}} \beta_{\text{R}}^{5-n} g^n \left( \frac{3-s}{n-s} \right)^3 \\ &\quad \left. \times (t' + t_i)^{\frac{2n+6s-n-15}{n-s}} \theta(t_{\text{RS,*}} - t') \right] dt', \end{aligned} \quad (17)$$

The final observed flux can be calculated by combining Eqs. (16) & (17):

$$F(t, \nu, P) = F_{\nu, \text{AG}}(t) + F_{\nu, \text{ej}}(t, t_{0,1}) + \frac{L_{t, \text{IPSN}}(t, t_{0,2})}{4\pi D_L^2} \quad (18)$$

where  $P$  is set a free parameters as specified in §4,  $t_{0,1}$  and  $t_{0,2}$  are the onset time of the two components.  $F_{\nu, \text{AG}}$  includes the standard afterglow component using an external forward shock model following the Python *afterglowpy* module (Ryan et al. 2020), as well as the magnetar spin-down energy contribution, which accounts for the shallow decay in X-ray. Eq. (18) can be directly compared with observational data through a Monte-Carlo fit (§4).

#### 4. THE FIT

The next step is to test our model with the observational data. To do so, we first collect all available observational data in the following energy band:

- $\gamma$ -ray. Following Zhang et al. (2021), GRB 200826A is shown as a short-duration burst with  $T_{90} = 0.96^{+0.05}_{-0.08}$  s at 10 – 800 keV band, with an isotropic energy of  $(7.09 \pm 0.28) \times 10^{51}$  erg.
- X-ray. Swift/XRT slewed to the direction of GRB 200826A at  $\sim 6 \times 10^4$  s after the trigger time of Fermi/GBM. The X-ray Data are obtained from

**Table 1.** Observations of optical counterpart of GRB 200826A

$\delta t(\text{day})$	Telescope	Band	System	Magnitude*	Flux Density ( $\mu\text{Jy}$ )	Ref.
Optical counterpart						
0.21	Zwicky Transient Facility	g	AB	$20.64 \pm 0.05$	$20.14^{+0.74}_{-0.71}$	(1)
0.23	Zwicky Transient Facility	r	AB	$20.55 \pm 0.05$	$21.88^{+0.89}_{-0.86}$	(1)
0.28	Zwicky Transient Facility	g	AB	$20.74 \pm 0.17$	$18.37^{+2.51}_{-2.15}$	(1)
0.77	Kitab-ISON RC-36	CR	AB	$> 20.3$	$< 27.54$	(3)
1.15	Zwicky Transient Facility	g	AB	$22.75 \pm 0.26$	$2.88^{+0.78}_{-0.61}$	(1)
1.22	Zwicky Transient Facility	r	AB	$> 21.16$	$< 12.47$	(1)
1.29	Zwicky Transient Facility	g	AB	$> 20.99$	$< 14.59$	(1)
1.74	Kitab-ISON RC-36	CR	AB	$> 20.5$	$< 22.91$	(3)
1.79	Swift/UVOT	white/(170-650 nm)	AB	$21.57 \pm 0.13$	$8.55^{+0.83}_{-0.74}$	(2)
2.18	Large Binocular Telescope	g	AB	$22.74 \pm 0.07$	$2.91^{+0.16}_{-0.15}$	(5)
2.18	Large Binocular Telescope	r	AB	$22.00 \pm 0.07$	$5.75^{+0.33}_{-0.31}$	(5)
2.27	LCOGT	r	AB	$> 23.30$	$< 1.74$	(8)
2.28	LCOGT	g	AB	$> 23.41$	$< 1.57$	(8)
3.23	Lowell Discovery Telescope	r	AB	$24.46 \pm 0.12$	$0.60^{+0.06}_{-0.07}$	(4)
3.99	Gran Telescopio Canarias	r	AB	$> 24.9$	$< 0.40$	(8)
28.28	Gemini-North 8-meter telescope/GMOS-N	i	AB	$25.45 \pm 0.25$	$0.24^{+0.06}_{-0.05}$	(7)
28.28	Gemini-North 8-meter telescope/GMOS-N	r	AB	$> 25.6$	$< 0.21$	(7)
31.81	TNG telescope	r	AB	$> 24.8$	$< 0.44$	(6)
32.81	LBT telescope /MODS	r	AB	$> 24.8$	$< 0.44$	(6)
46.11	Gemini-North 8-meter telescope/GMOS-N	i	AB	$> 25.4$	$< 0.25$	(7)
46.11	Gemini-North 8-meter telescope/GMOS-N	r	AB	$> 25.5$	$< 0.23$	(7)
72.05	LCOGT network observatory	i	AB	$> 22.7$	$< 3.02$	(8)
72.48	Lijiang 2.4-meter telescope	g	AB	$> 22.58$	$< 3.37$	(8)
72.48	Lijiang 2.4-meter telescope	r	AB	$> 22.07$	$< 5.40$	(8)
72.48	Lijiang 2.4-meter telescope	i	AB	$> 21.81$	$< 6.85$	(8)

(1) GCN Circular 28295 T. Ahumada et al.

(2) GCN Circular 28300 A. D’Ai et al.

(3) GCN Circular 28306 S. Belkin et al.

(4) GCN Circular 28312 B. S.Dichiara et al.

(5) GCN Circular 28319 B. Rothberg et al.

(6) GCN Circular 28949 A.Rossi et al.

(7) GCN Circular 29029 T. Ahumada et al.

(8) This work

\* Corrected for foreground Galactic extinction on the line of sight (Schlafly & Finkbeiner 2011).

the Swift/XRT repository<sup>2</sup> (Evans et al. 2007, 2009) and are plotted in the middle panel Figure 2.

- **Optical.** The first optical counterpart is obtained by Zwicky Transient Facility (ZTF) at  $\sim 0.2$  days (Ahumada et al. 2020) and the host galaxy is confirmed with redshift  $z = 0.7481 \pm 0.0003$  (Rothberg et al. 2020). An optical flare is observed by Large Binocular Telescope (LBT) (Rothberg et al. 2020) at 2.18 days. We carried out our observations in r-band with Las Cumbres Observatory Global Telescope (LCOGT) and obtained several upper-limits around 2.27 days. Ahumada et al. (2021) reported a series of i-band observations from Gemini-North 8-meter telescope, and measured an optical bump with  $M_i = 25.45 \pm 0.25$  AB mag at  $t \sim 28.28$  days. All those data, as well as those reported in GCN circulars<sup>3</sup> by multiple facilities, including Telescopio Nazionale Galileo (TNG), Gran Telescopio Canarias (GTC), and Lowell Discovery Telescope (LDT), are all collected and listed in Table 1.
- **Radio.** As reported in Alexander et al. (2020), VLA observed the position of GRB 200826A 2.28 days after GBM trigger at a mean frequency of 6 GHz. A radio source was detected with a flux density of  $\sim 40 \mu\text{Jy}$  at the position of GRB 200826A. Rhodes et al. (2021) carried out a survey of enhanced Multi Element Remotely Linked Interferometer Network (eMERLIN) observations of GRB 200826A. They obtained two radio detections of  $93 \pm 16 \mu\text{Jy}$  and  $68 \pm 8 \mu\text{Jy}$  at  $4.92 \pm 0.5$  and  $6.4 \pm 0.9$  days, respectively, and an upper-limit of  $F_\nu < 34 \mu\text{Jy}$  at  $8.7 \pm 1.9$  days. The upgraded Giant Metrewave Radio Telescope (uGMRT) performed an observation 14.47 days after the burst. The central frequency is 1.25 GHz, and the radio emission reported was below a  $3\sigma$  upper-limit of  $48.6 \mu\text{Jy}/\text{beam}$ . All those numbers are plotted in Figure 2 and taken into account in our fit.

We then fit our model (Eq. (18)) to above observational data using a self-developed Bayesian Monte-Carlo fitting package, *McEasyFit* (Zhang et al. 2015), which ensures that the reliable best-fit parameters and their uncertainties can be realistically determined by the converged MC chains. The free parameters as well as their allowed ranges are listed in Table 2. The priors of the

<sup>2</sup> [https://www.swift.ac.uk/xrt\\_curves/00021028/](https://www.swift.ac.uk/xrt_curves/00021028/)

<sup>3</sup> <https://gcn.gsfc.nasa.gov/other/200826A.gcn3>

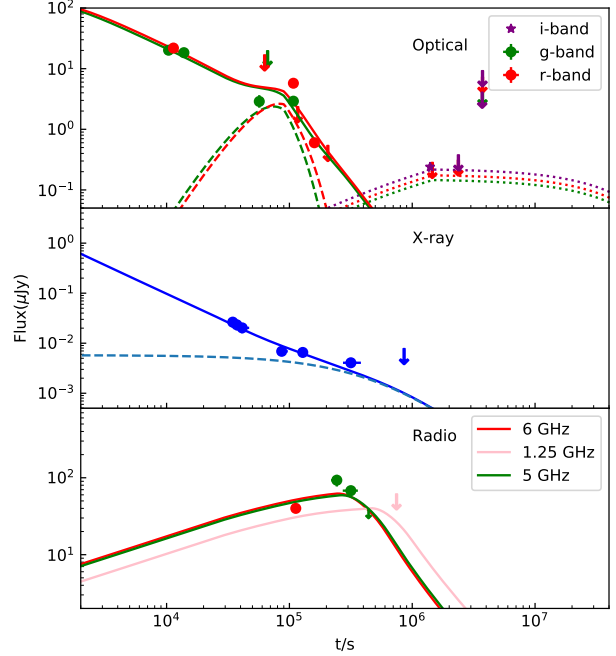


**Figure 2.** Multi-wavelength observation data of GRB 200826A over-plotted with our model using the best-fit parameters. *Top:* Data points show the optical observations. Solid line show the model prediction using the best-fit parameters in Table 2. The dashed lines show the merger-nova-like components and the dotted lines show the late-time SN-bump-like component. *Middle:* Data points show the X-ray observations by Swift/XRT. Solid line show the model prediction and dashed line shows the shallow-decay component powered by the magnetar. *Bottom:* Radio afterglow (filled circles) overplotted with the best-fit models (solid lines).

fitting free parameters are set to uniform (those listed as “parameter name” in Table 2) or log uniform (those listed as “log parameter name” in Table 1) distributions in physically allowed large ranges (see below). Our model successfully fit the data. The best-fit parameters as well as their constraints are listed in Table 2 and plotted in Figure 3. The model predictions using the best-fit parameters are over-plotted in Figure 2.

Our fit highlights the following physical constraints of the system:

- $\xi$ . The best-fit value of the energy ejection ratio,  $\xi$ , is constrained at  $0.54^{+0.06}_{-0.29}$ , indicating that half of the spin-down energy injects into the ejecta.
- $\kappa$ . Our result shows the opacity of the ejecta is  $\kappa = 50.22^{+1.17}_{-32.00}$ . Such a large opacity suggest the

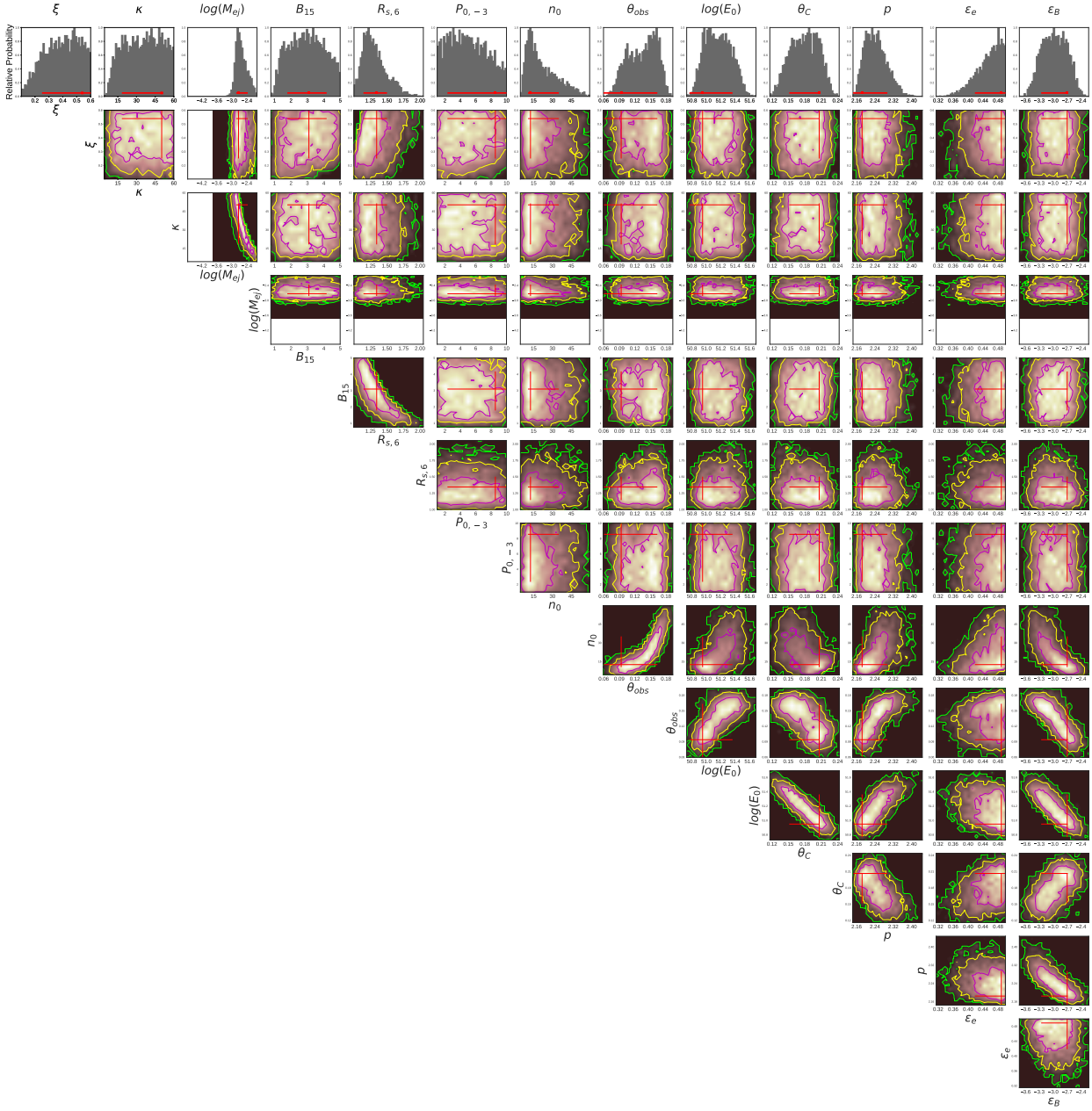


Figure 3. Parameter constraints of our model fit using *McEasyFit*.

**Table 2.** Best-fit parameters and their uncertainties of our model to the multi-wavelength data

Parameters	Range	Best-Fit
$\xi$	[0.1, 0.6]	$0.54^{+0.06}_{-0.29}$
$\kappa$	[0.1, 60]	$50.22^{+1.17}_{-32.00}$
$\log(M_{\text{ej}})(M_{\odot})$	[-5.0, -2.0]	$-2.74^{+0.37}_{-0.09}$
$B_{15}$ (G)	[0.1, 5.0]	$3.09^{+1.08}_{-1.31}$
$R_{s,6}$ (cm)	[1.0, 3.0]	$1.34^{+0.16}_{-0.2}$
$P_{0,-3}$ (s)	[1.0, 10]	$8.55^{+1.44}_{-6.22}$
$n_0$	[0.1, 60]	$12.50^{+22.64}_{-2.02}$
$\theta_{\text{obs}}$ (rad)	[0.0, 0.2]	$0.09^{+0.07}_{-0.03}$
$\theta_C$ (rad)	[0.05, 0.4]	$0.21^{+0.0005}_{-0.05}$
$\log(E_0)$ (erg)	[50, 53]	$50.95^{+0.41}_{-0.18}$
p	[2.01, 2.99]	$2.18^{+0.11}_{-0.04}$
$\epsilon_e$	[0.01, 0.5]	$0.49^{+0.01}_{-0.07}$
$\epsilon_B$	[-5.0, -2.0]	$-2.70^{+0.01}_{-0.56}$

ejecta should be rich in heavy elements (Yu et al. 2018; Tanaka et al. 2020), possibly brought by the effect of rebound shock.

- $M_{\text{ej}}$ . With  $M_{\text{ej}} = 0.0034^{+0.0046}_{-0.0006} M_{\odot}$ , the mass of the ejecta is found similar to the result of NS-NS merger simulation (Hotokezaka et al. 2013).
- $n_0$ . The interstellar medium density is constrained at  $n_0 = 12.5^{+22.64}_{-2.02} \text{ cm}^{-3}$ . Such a large value is consistent with the observational fact that the burst is located in the host galaxy with a small offset (Zhang et al. 2021), likely a denser area with higher star-formation rate, yet it allows the possibility of forming a WD-NS system (Zhong & Dai 2020; Toonen et al. 2018).
- $\theta_C$  &  $\theta_{\text{obs}}$ . The jet-core angle and the observer angle are constrained at  $\theta_C = 12.03^{+0.03}_{-2.86}$  degrees and  $\theta_{\text{obs}} = 5.16^{+4.01}_{-1.72}$  degrees, respectively, suggesting an on-axis observation of typical GRB jet.
- Neutron star properties. Our fit constrains a NS with a magnetic field of  $3.09^{+1.08}_{-1.31} \times 10^{15}$  G, a radius of  $1.34^{+0.16}_{-0.20} \times 10^6$  cm, and rotating period of  $8.55^{+1.44}_{-6.22}$  ms, fully consistent the magnetar-powered GRB central engine. We also derive the corresponding magnetic dipole radiation is characterized by  $t_{\text{sd}} = 6 \times 10^5$  s, and  $L_{\text{sd},0} = 10^{44.7} \text{ erg s}^{-1}$ .

- A merger-nova-like component. The best-fit of our model yields a significant optical bump as well as an X-ray shallow decay component at  $\sim 2-3$  days, as plotted with dashed lines in the top two panels in Figure 2.

- The supernova-like optical bump. Our model successfully explained the optical bump at 28.28 days as an IPSN with the following key settings in Eq. (17): (1) compact profile  $n = 6$ . (2) the power-law exponent for the CBM shell density profile  $s = 2$ . (3) Some other related parameters  $A$ ,  $\beta_F$  and  $\beta_R$  were given in Table 1 of Chevalier (1982). (4) The mass of compact CBM is set to  $M_{\text{CBM}} = 0.5 M_{\odot}$  with density of  $\rho_{\text{CBM}} = 1.0 \times 10^{-14} \text{ g cm}^3$  (Metzger 2012; Margalit & Metzger 2016). (5) The radius when the ejecta collide with CBM shell is at  $\sim 10^{15}$  cm. (6) The optical depth of CBM is  $\tau_{\text{Thomson}} \approx \kappa_0 M_{\text{CBM}} / 4\pi R^2 > 1$ , where  $R$  is the radius of the disk wind shell and  $\kappa_0$  is the Thomson scattering opacity of the CBM which is set to  $\kappa_0 = 0.33 \text{ cm}^2 \text{ g}^{-1}$ . We notice that  $R \lesssim 5 \times 10^{15}$  cm to meet the optical thin condition. (7) The photosphere radius of the IPSN is set to  $R_{\text{ph}} = 2.0 \times 10^{15} \text{ cm}$ .

## 5. SUMMARY AND DISCUSSIONS

In this *Letter*, we introduce the collapse of a TZIO as the progenitor of the peculiar short-duration GRB 200826A. The model naturally explains the collapsar-like character of the burst. The accretion timescale calculated through large WD-density of TZIO envelope is found consistent with the short-duration of GRB 200826A. By fitting our model to the observational data, we found that the final product of such collapse is likely a magnetar, which injects additional dipole radiation to the ejecta and powers a bump in optical and a shallow decay in X-ray at  $\sim 2-3$  days. Additionally, the interaction between the ejecta and disk wind shell successfully explains the late-time optical bump at  $\sim 28.28$  days.

The event rate of WD-NS mergers is  $\sim 0.5 - 1 \times 10^4 \text{ Gpc}^{-3} \text{ yr}^{-1}$  (Thompson et al. 2009; Paschalidis et al. 2011b), or as lower as  $\sim 0.7 - 7 \times 10^3 \text{ Gpc}^{-3} \text{ yr}^{-1}$  in the near cosmos (Liu 2018). A non-negligible fraction of those mergers can undergo the UMT process (Bobrick et al. 2017) and produce TZIOs. Whether or not all of those TZIOs can further collapse and generate GRB 200826A-like events remains an open question. Nevertheless, discoveries of similar events in the future or the existing GRB samples can shed some light on this new class of GRB events and the fate of the WD-NS mergers.



1 We thank H. Gao, R.-F. Sheng, Y. Shao for helpful dis-  
 2 cussions on the paper. B.B.Z acknowledges support by  
 3 Fundamental Research Funds for the Central Univer-  
 4 sities (14380046), the National Key Research and De-  
 5 velopment Programs of China (2018YFA0404204), the  
 6 National Natural Science Foundation of China (Grant  
 7 Nos. 11833003, U2038105), the science research grants  
 8 from the China Manned Space Project with NO.CMS-  
 9 CSST-2021-B11, and the Program for Innovative Tal-  
 10 ents, Entrepreneur in Jiangsu.

## REFERENCES

- Ahumada, T., Anand, S., Stein, R., et al. 2020, GRB Coordinates Network, Circular Service, No. 28295, 28295
- Ahumada, T., Singer, L. P., Anand, S., et al. 2021, *Nature Astronomy*. doi:10.1038/s41550-021-01428-7
- Alexander, K. D., Fong, W., Paterson, K., et al. 2020, GRB Coordinates Network, Circular Service, No. 28302, 28302
- Bruenn, S. W. 1985, *ApJS*, 58, 771. doi:10.1086/191056
- Beaudet, G., Petrosian, V., & Salpeter, E. E. 1967, *ApJ*, 150, 979. doi:10.1086/149398
- Belczynski, K., Bulik, T., & Rudak, B. 2002, *ApJ*, 571, 394. doi:10.1086/339860
- Bobrick, A., Davies, M. B., & Church, R. P. 2017, *MNRAS*, 467, 3556. doi:10.1093/mnras/stx312
- Chatzopoulos, E., Wheeler, J. C., & Vinko, J. 2012, *ApJ*, 746, 121. doi:10.1088/0004-637X/746/2/121
- Chevalier, R. A. 1982, *ApJ*, 258, 790. doi:10.1086/160126
- Dong, D. Z., Hallinan, G., Nakar, E., et al. 2021, *Science*, 373, 1125. doi:10.1126/science.abg6037
- Evans, P. A., Beardmore, A. P., Page, K. L., et al. 2007, *A&A*, 469, 379. doi:10.1051/0004-6361:20077530
- Evans, P. A., Beardmore, A. P., Page, K. L., et al. 2009, *MNRAS*, 397, 1177. doi:10.1111/j.1365-2966.2009.14913.x
- Hotokezaka, K., Kiuchi, K., Kyutoku, K., et al. 2013, *PhRvD*, 87, 024001. doi:10.1103/PhysRevD.87.024001
- Huang, Y. F., Dai, Z. G., & Lu, T. 2000, *MNRAS*, 316, 943. doi:10.1046/j.1365-8711.2000.03683.x
- Kasen, D. & Bildsten, L. 2010, *ApJ*, 717, 245. doi:10.1088/0004-637X/717/1/245
- Kotera, K., Phinney, E. S., & Olinto, A. V. 2013, *MNRAS*, 432, 3228. doi:10.1093/mnras/stt680
- Lasky, P. D., Leris, C., Rowlinson, A., et al. 2017, *ApJL*, 843, L1. doi:10.3847/2041-8213/aa79a7
- Liu, X. 2018, *Ap&SS*, 363, 242. doi:10.1007/s10509-018-3462-3
- Margalit, B. & Metzger, B. D. 2016, *MNRAS*, 461, 1154. doi:10.1093/mnras/stw1410
- Metzger, B. D. 2012, *MNRAS*, 419, 827. doi:10.1111/j.1365-2966.2011.19747.x
- Middleditch, J. 2004, *ApJL*, 601, L167. doi:10.1086/382074
- Paschalidis, V., Liu, Y. T., Etienne, Z., et al. 2011, *PhRvD*, 84, 104032. doi:10.1103/PhysRevD.84.104032
- Paschalidis, V., Etienne, Z., Liu, Y. T., et al. 2011, *PhRvD*, 83, 064002. doi:10.1103/PhysRevD.83.064002
- Rhodes, L., Fender, R., Williams, D. R. A., et al. 2021, *MNRAS*, 503, 2966. doi:10.1093/mnras/stab640
- Rothberg, B., Kuhn, O., Veillet, C., et al. 2020, GRB Coordinates Network, Circular Service, No. 28319, 28319
- Ryan, G., van Eerten, H., Piro, L., et al. 2020, *ApJ*, 896, 166. doi:10.3847/1538-4357/ab93cf
- Schlaflly, E. F. & Finkbeiner, D. P. 2011, *ApJ*, 737, 103. doi:10.1088/0004-637X/737/2/103
- Tanaka, M., Kato, D., Gaigalas, G., et al. 2020, *MNRAS*, 496, 1369. doi:10.1093/mnras/staa1576
- Thompson, T. A., Kistler, M. D., & Stanek, K. Z. 2009, arXiv:0912.0009
- Toonen, S., Perets, H. B., Igoshev, A. P., et al. 2018, *A&A*, 619, A53. doi:10.1051/0004-6361/201833164
- van Riper, K. A. 1982, *ApJ*, 257, 793. doi:10.1086/160032
- van Riper, K. A. & Lattimer, J. M. 1981, *ApJ*, 249, 270. doi:10.1086/159285
- Z.-G. 2019, *ApJL*, 879, L7. doi:10.3847/2041-8213/ab2980
- Yang, J., Chand, V., Zhang, B.-B., et al. 2020, *ApJ*, 899, 106. doi:10.3847/1538-4357/aba745
- Yu, Y.-W., Zhang, B., & Gao, H. 2013, *ApJL*, 776, L40. doi:10.1088/2041-8205/776/2/L40
- Yu, Y.-W., Liu, L.-D., & Dai, Z.-G. 2018, *ApJ*, 861, 114. doi:10.3847/1538-4357/aac6e5
- Zhang, B. 2011, *Comptes Rendus Physique*, 12, 206. doi:10.1016/j.crhy.2011.03.004
- Zhang, B.-B., van Eerten, H., Burrows, D. N., et al. 2015, *ApJ*, 806, 15. doi:10.1088/0004-637X/806/1/15

Zhang, B.-B, Liu, Z.-K, Peng, Z.-K., et al. *Nat Astron*  
(2021). doi:10.1038/s41550-021-01395-z

Zhong, S.-Q. & Dai, Z.-G. 2020, *ApJ*, 893, 9.  
doi:10.3847/1538-4357/ab7bdf